This is a preprint of the following published article:
Poulos, A., & Miranda, E. (2023). Modification of ground-motion models to estimate orientation-dependent horizontal response spectra in strike-slip earthquakes. *Bulletin of the Seismological Society of America*. Advance online publication. https://doi.org/10.1785/0120230084

Modification of ground-motion models to estimate orientation-dependent horizontal response spectra in strike-slip earthquakes

Alan Poulos*[1] and Eduardo Miranda[1]

[1]Department of Civil and Environmental Engineering, Stanford University, Stanford, California, U.S.A.

Abstract

A model to estimate 5%-damped response spectra of horizontal components at specific orientations is presented. The model, which accounts explicitly for directionality, is based on prior research by the authors that identified that the orientation of maximum horizontal spectral response at a site in strike-slip earthquakes tends to occur at or close to the transverse orientation with respect to the epicenter. By using a database of 1962 ground motions recorded in shallow crustal earthquakes with strike-slip faulting, it is shown that there is a significantly larger probability of exceeding orientation-independent RotD50 intensities in the transverse orientation than in the radial orientation. Furthermore, the results indicate that, on average, spectral responses in the transverse orientation are significantly larger than those in the radial orientation and that these differences become more significant as the period of the oscillator increases. For example, spectral responses in the transverse orientation are, on average, 12% larger than those in the radial orientation for 1-s oscillators and are 78% larger for 10-s oscillators. A period- and orientation-dependent model is developed and calibrated to estimate 5%-damped response spectral ordinates at specific orientations by modifying orientation-independent RotD50 intensities. The proposed orientation-dependent model can be used to explicitly account for directionality by modifying means and standard deviations of any ground motion model that estimates RotD50 response spectral ordinates for strike-slip earthquakes to obtain probability distributions of response spectral ordinates but now at specific horizontal orientations.

Introduction

Earthquake ground motion intensity is usually characterized by 5%-damped horizontal response spectra for earthquake engineering purposes. These spectral responses exhibit significant variation

*Corresponding author: apoulos@stanford.edu

within the horizontal plane, that is, they depend on the azimuth at which they are recorded or computed from recorded components, a phenomenon known as directionality. Ground motion models (GMMs) and earthquake-resistant design procedures usually neglect this variation with changes in orientation by using a single value of intensity representative of all azimuths, such as the geometric mean between the intensities at the two as-recorded orientations or the median intensity from all azimuths, usually referred to as RotD50 (Boore, 2010).

Empirical studies have shown that spectral acceleration directionality is significant and increases with period (e.g., Hong and Goda, 2007; Poulos and Miranda, 2022a). For example, the 5%-damped maximum horizontal spectral acceleration from all azimuths (i.e., RotD100) is, on average, 55% and 100% higher than the spectral acceleration in the corresponding perpendicular orientation for periods of 1 and 10 s, respectively (Poulos et al., 2022). In these types of studies, spectral accelerations are characterized as a function of their angle with respect to the orientation in which maximum horizontal spectral response occurs, i.e., they study their variation with respect to the orientation RotD100. However, predicting this orientation at a given site for a future earthquake scenario remains challenging.

Significant attention has been given in the literature to directionality caused by directivity effects in the near-field of crustal earthquakes that may produce pulse-like ground motions. For example, Somerville et al. (1997) found that at periods longer than 0.6 s, spectral accelerations in the strike-normal orientation tend to be higher than average in the near-fault region. They attributed this to the radiation pattern of shear waves caused by the shear dislocation occurring on the fault that tends to produce a distinct large pulse in an orientation perpendicular to the fault plane (Somerville et al., 1997). However, subsequent studies have shown that, even in the near-fault region, the orientation of maximum spectral acceleration can differ significantly from the strike-normal orientation (e.g., Howard et al., 2005; Watson-Lamprey and Boore, 2007; Shahi and Baker, 2014) and that the tendency of the maximum intensities to occur at or near to the strike-normal orientation disappears fairly fast as the source-to-site distance increases, being no better than a random orientation for rupture distances greater than approximately 5 km (Shahi and Baker, 2014).

Ground motion directionality has also been attributed to several other causes that can occur at any distance to the source, such as topographic irregularities (e.g., Spudich et al., 1996), local geologic heterogeneities (e.g., Bonamassa and Vidale, 1991), and basin edge effects (e.g., Heresi et al., 2020). However, despite these studies, systematic procedures to improve the prediction of the RotD100 orientation are currently unavailable.

Recently, Poulos and Miranda (2023) studied the orientation of maximum horizontal spectral response in 5065 ground motion records from shallow crustal earthquakes and showed that, for strike-slip earthquakes, the orientation of maximum spectral response tends to occur at or close to the transverse orientation (i.e., the orientation that is perpendicular to an imaginary line segment joining the site to the epicenter) and that this tendency increases as the period becomes longer. This paper builds upon this finding by studying how spectral accelerations at specific orientations depend on the angle with respect to the transverse orientation. Probabilistic expressions are then developed to enable the transformation of 5%-damped median spectral accelerations (i.e., RotD50) to spectral accelerations in any specific orientation, therefore removing the need to predict the orientation of maximum spectral acceleration. This model can be used together with a GMM that estimates 5%-damped RotD50 spectral accelerations to account for the predominance of polarization along the transverse orientation in strike-slip earthquakes. Finally, probability distributions are

fitted to the ratio between spectral accelerations at a fixed horizontal orientation and the RotD50 spectral acceleration at different periods and angles with respect to the transverse orientation.

Orientation of maximum spectral response

Horizontal ground motions are usually recorded in two orthogonal directions. Therefore, both records can be used to compute the bidirectional response of a linear elastic single-degree-of-freedom (SDOF) system with a specific period of vibration and damping ratio (assumed to be 5% in this study). Spectral accelerations at all possible horizontal directions (azimuths) can then be obtained by computing the maximum absolute response within the corresponding direction (see, for example, Poulos and Miranda, 2022b). The maximum horizontal spectral acceleration, known as RotD100, occurs at a record- and period-dependent orientation.

Figure 1 shows the RotD100 orientations computed for 10-s oscillators at stations (indicated by small circles) that recorded the 2019 M_w 7.1 Ridgecrest earthquake using a black line behind each circle. The ground motion records were obtained from the database compiled by Rekoske et al. (2020). Visually, we can observe that these orientations tend to be close to the transverse orientation, that is, an orientation perpendicular to an imaginary line segment joining the epicenter to the site of interest (in this case a recording station). The absolute value of the angular difference between these two orientations (i.e., transverse orientation and the orientation of RotD100) is denoted by $|\alpha|$, and its value at each site is given by the color of each corresponding circle. $|\alpha|$ is, by definition, always between 0° and 90°, and its probability distribution should be relatively uniform if the transverse orientation has no predictive power (i.e., the maximum spectral response is equally likely to occur in any orientation). However, the histogram presented in the lower left corner of Figure 1 shows that the RotD100 orientations are much more likely to occur closer to the transverse orientation than would be expected if $|\alpha|$ were uniformly distributed, with a mean angular distance of only 21.4°, which is much lower than that of a uniform distribution, where this mean would be 45°.

Poulos and Miranda (2023) showed that the behavior presented in Figure 1 from the 2019 M_w 7.1 Ridgecrest earthquake, in which the orientations of RotD100 tend to occur at or close to the transverse orientation, is characteristic of ground motion records from strike-slip earthquakes. Furthermore, they show that this tendency of orientation and level of polarization becomes more important as the period increases, with the expected value of $|\alpha|$ being approximately 39° and 23° for periods of 1 s and 10 s, respectively, angles that are 13% and 49% smaller than those that would occur if the transverse orientation had no predictive power to estimate the orientation in which RotD100 occurs (Poulos and Miranda, 2023). On the other hand, the same study found that records from reverse earthquakes in the NGA-West2 ground motion database do not exhibit this behavior.

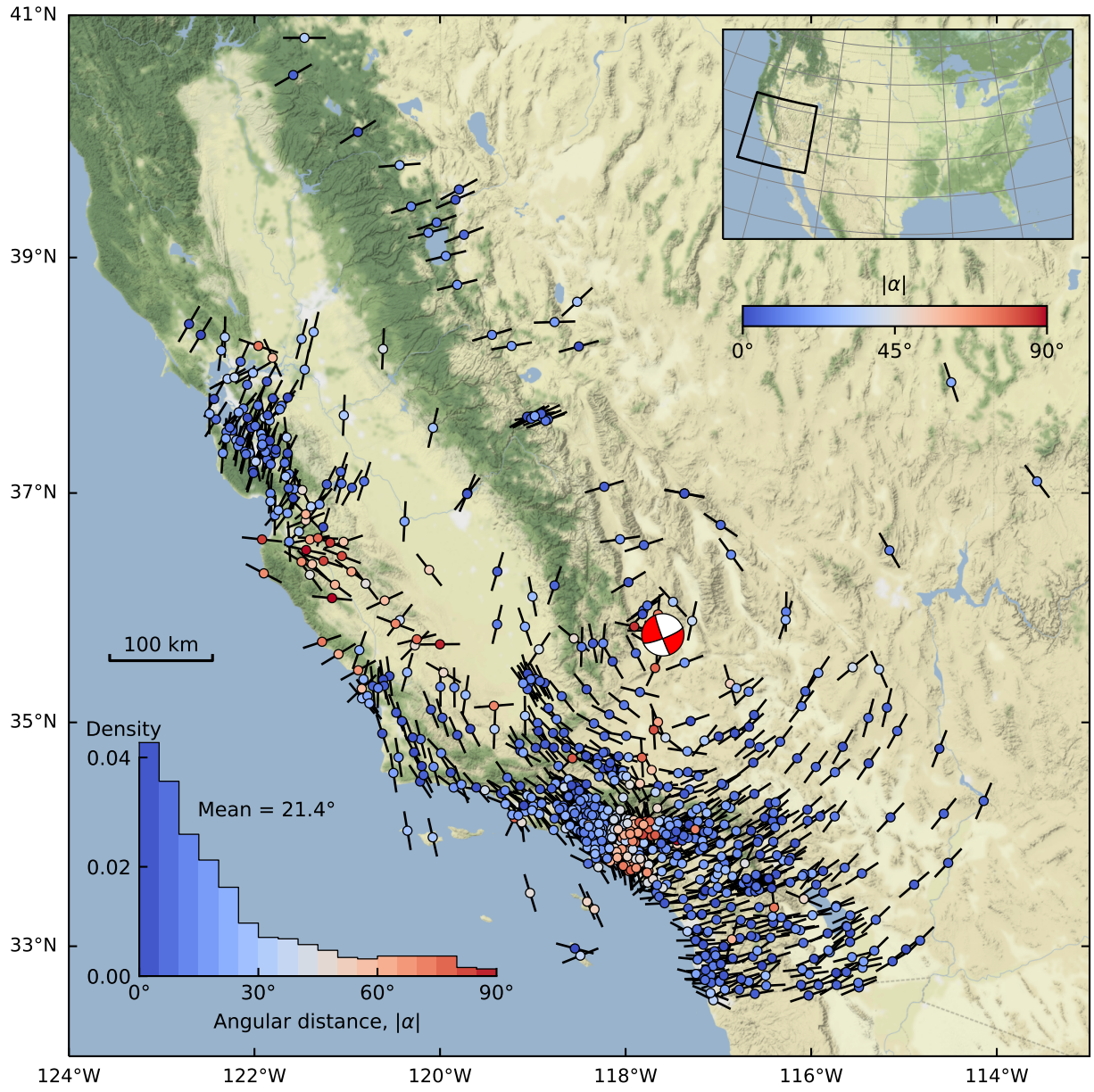

Figure 1: Orientations of maximum horizontal spectral response of oscillators with a period of 10 s computed for ground motion records from the 2019 M_w 7.1 Ridgecrest earthquake. The color of the circles represents the angular distance to the transverse orientation at each site. The upper right inset shows the location of the map within the contiguous United States. The lower left inset shows the empirical probability density of angular distance $|\alpha|$.

Spectral responses in the transverse and radial orientations

As explained in the previous section, the orientation in which the maximum spectral acceleration tends to occur is close to the transverse orientation for ground motions from strike-slip earthquakes, which leads to spectral accelerations in the transverse orientation being, on average, larger than

the median intensity from all orientations. Conversely, on average, spectral accelerations in the radial orientation are lower than the median intensity from all orientations. Consequently, the intensity in the transverse orientation can be considerably stronger than in the radial orientation. To illustrate this, Figure 2 presents the directionality of a ground motion from the 2010 M_w 7.2 El Mayor-Cucapah earthquake recorded in the Anaheim station (record sequence number 5919 in the NGA-West2 database), which was located at a rupture distance of 236 km. Figure 2a shows the bidirectional response of a 6-s linear elastic oscillator by presenting its relative displacement hodogram. The same figure also presents the spectral displacements in all directions using a polar representation, where the spectral displacement at a given direction corresponds to the distance from the spectral displacement curve to the origin. It can be seen that, for this example, the orientation of maximum response (RotD100), which is presented by a black line in Figure 2a, is much closer to the transverse orientation than to the radial orientation. Consequently, as shown in Figure 2c, the relative displacement history is much larger in the transverse orientation than in the radial orientation, which leads to the peak relative displacement (i.e., the spectral displacement) also being much larger in the transverse orientation than in the radial orientation (3.38 times larger for this particular records and period).

The responses of oscillators of all periods between 0 and 10 s for the same example ground motion record are summarized by the acceleration and displacement spectra shown in Figures 2b and 2d, respectively. The figures represent, at any period, the range of spectral responses with changes in orientation by a shaded area and highlight the response spectrum in the transverse ($\alpha = 0°$) and radial ($|\alpha| = 90°$) orientations. For this particular record, the spectra do not depend very much on the orientation for periods shorter than 4 s. However, for periods longer than roughly 4 s, the range of spectral responses becomes much wider indicating that the response of the oscillator tends to be much more polarized despite the recording station being very far away from the epicenter. At all these long periods, the response spectrum in the transverse orientation is significantly larger and much closer to the RotD100 spectrum than the response spectrum in the radial orientation. Moreover, median spectral responses from all orientations (RotD50), which are used in most recent GMMs and are depicted in the figure by dashed lines, are lower than spectral responses in the transverse orientation and higher than spectral responses in the radial orientation for all periods. Strong polarizations like those observed here have often been attributed to directivity effects. However, that is unlikely in this case, given that the recording station was more than 200 km from the earthquake rupture. Poulos and Miranda (2023) found that orientations of maximum intensity at or close to the transverse orientation for strike-slip events is consistent with the polarization of SH waves from theoretical double couple point sources within a homogeneous propagation medium.

To study the observations of Figure 2 in a more general case and obtain statistically significant results, this work used a large number of recorded ground motions corresponding to a subset of the NGA-West2 ground motion database (Ancheta et al., 2014). The selected records corresponded to those recorded from earthquakes with magnitudes equal to or greater than 5.0; at stations with NEHRP site classes B, C, or D (i.e., those with a time-weighted average shear-wave velocity over the upper 30 m between 180 and 1500 m/s); and that reasonably represented free-field conditions following the criteria defined by Boore et al. (2014). The resulting subset contained 5,065 horizontal pairs of ground motions. Spectral accelerations were computed for all selected records at 32 periods between 0.01 and 10 s. RotD50 values were computed as the median of the spectral accelerations at non-redundant azimuths with 1° increments.

Figure 3 shows the probability that a spectral acceleration in the transverse orientation ex-

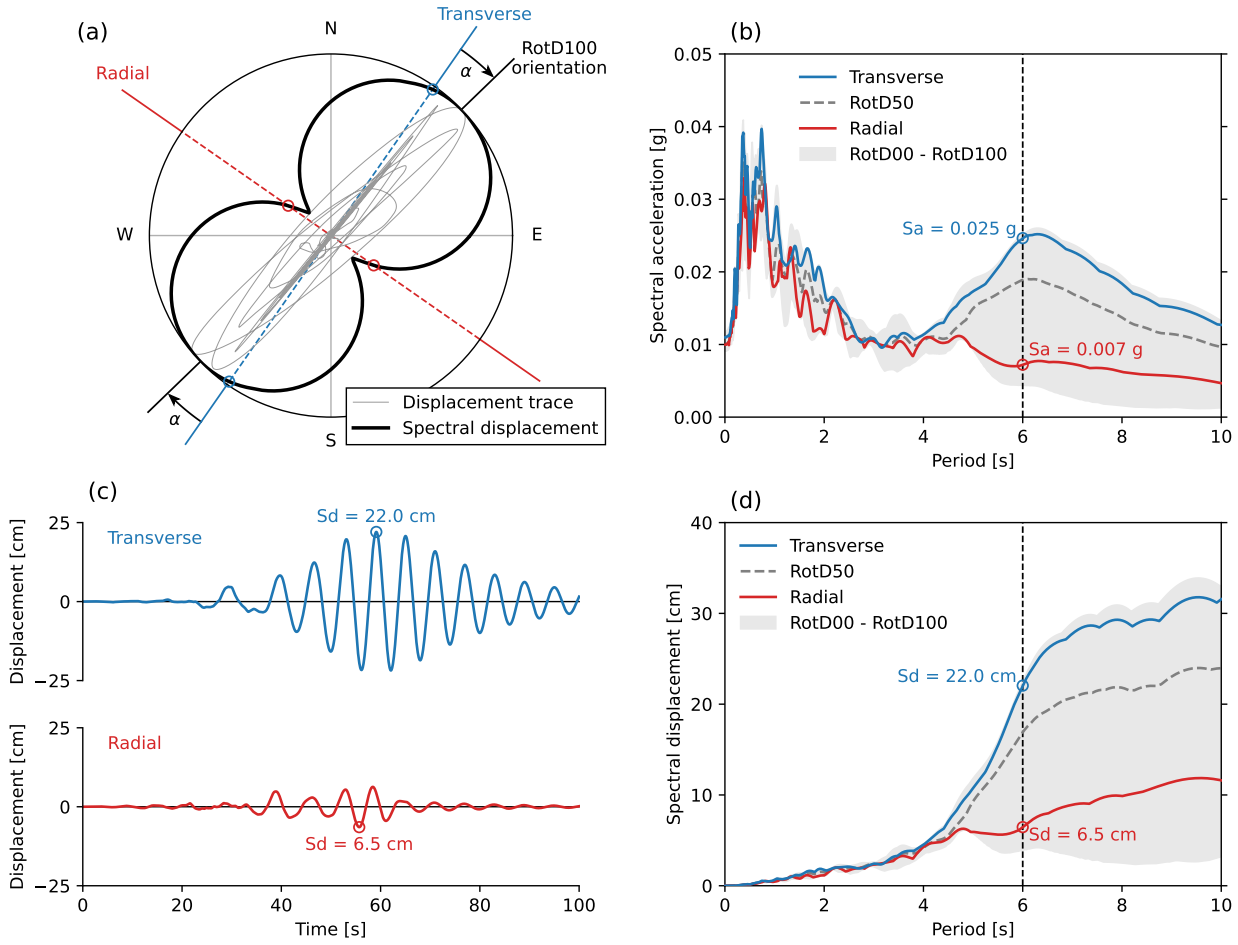

Figure 2: Example ground motion from the 2010 M_w 7.2 El Mayor-Cucapah earthquake recorded in the Anaheim station: (a) bidirectional horizontal displacement trace of a 6-s linear elastic oscillator, (b) spectral accelerations, (c) relative displacement response in transverse and radial orientations of a 6-s linear elastic oscillator, and (d) spectral displacements.

ceeds RotD50 and the probability that a spectral acceleration in the radial orientation exceeds RotD50. These probabilities were computed as the proportion of records in the set where RotD50 is exceeded and were calculated separately for records from strike-slip and reverse earthquakes. Records from normal-faulting earthquakes were not considered in this study due to their very low number in the NGA-West2 subset database. In the absence of a predominant orientation of maximum intensity, these probabilities would be expected to be close to 0.5, which is what occurs for records from reverse earthquakes. However, as expected based on the observations by Poulos and Miranda (2023), records from strike-slip earthquakes have a probability of exceeding RotD50 significantly higher than 0.5 in the transverse orientation and significantly lower than 0.5 in the radial orientation. Moreover, these differences tend to become more important as the period increases. For example, the exceedance probability for the transverse orientation is approximately 0.6 at 1 s and reaches 0.86 at 10 s. Figure 3 also presents 95% pointwise confidence bands of these exceedance probability estimations computed using bootstrapping (Efron and Tibshirani, 1993), showing that, for all periods, the differences in probabilities of exceeding RotD50 in the transverse

and radial orientations for the strike-slip case are statistically significant. These results indicate that, for strike-slip earthquakes, using RotD50 for earthquake-resistant design tends to underestimate intensities in the transverse orientation and overestimate intensities in the radial orientation.

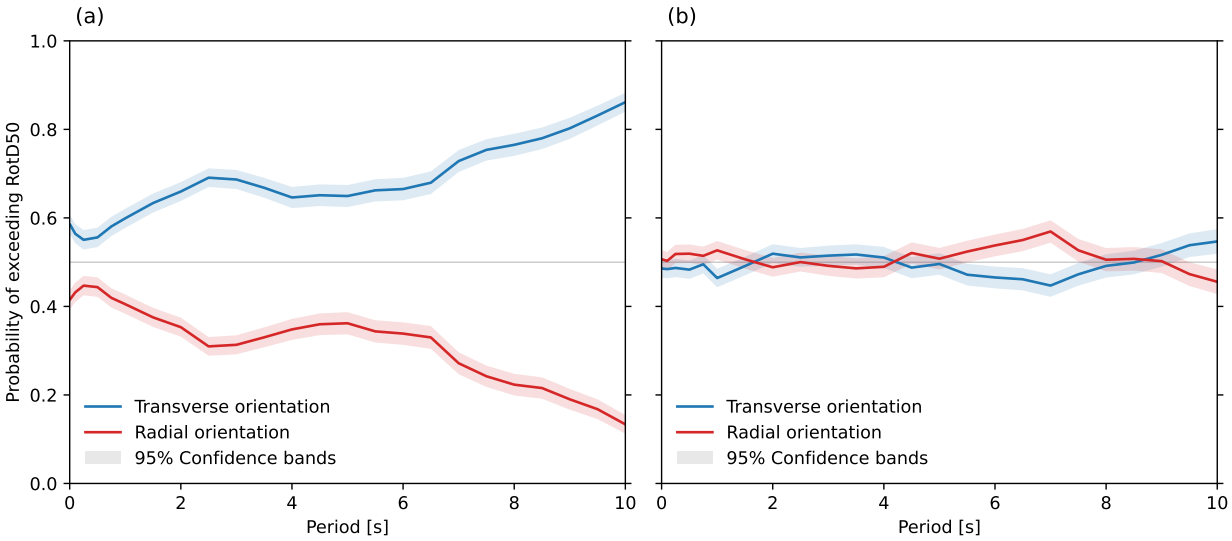

Figure 3: Probability that intensities in the transverse and radial orientations exceed the RotD50 intensity for ground motions from earthquakes with (a) strike-slip and (b) reverse style of faulting.

To quantify how much spectral accelerations in the transverse and radial orientations differ from RotD50, one can compute the ratios between these values, that is, $Sa_{\mathrm{T}}/Sa_{\mathrm{RotD50}}$ and $Sa_{\mathrm{R}}/Sa_{\mathrm{RotD50}}$, respectively. Figure 4 shows the mean and interquartile ranges of these ratios as a function of period for records from both strike-slip and reverse earthquakes. As shown in the figure, for all periods, mean $Sa_{\mathrm{T}}/Sa_{\mathrm{RotD50}}$ values are larger than one and mean $Sa_{\mathrm{R}}/Sa_{\mathrm{RotD50}}$ values are lower than one for strike-slip earthquakes. Thus, ground motion records from strike-slip earthquakes have spectral accelerations that are, on average, significantly larger in the transverse orientation than in the radial orientation, and this difference again becomes larger as the period increases. Indeed, a two-sample Kolmogorov-Smirnov test led to reject the hypothesis that the $Sa_{\mathrm{T}}/Sa_{\mathrm{RotD50}}$ and $Sa_{\mathrm{R}}/Sa_{\mathrm{RotD50}}$ samples are drawn from the same probability distribution at all periods for the strike-slip case, indicating that intensities in the transverse orientation are statistically different to those in the radial orientation. On the other hand, for ground motions from reverse earthquakes, the test could not reject the hypothesis for most of the studied periods, indicating that spectral accelerations in the transverse orientation seem not to be statistically different from those in the radial orientation. Figure 4 also shows mean ratios between intensities at an arbitrary orientation Sa_{Arb} and RotD50, which are slightly lower than one because the mean from all non-redundant orientations is, on average, slightly lower than the median (RotD50).

The possible dependence of $Sa_{\mathrm{T}}/Sa_{\mathrm{RotD50}}$ and $Sa_{\mathrm{R}}/Sa_{\mathrm{RotD50}}$ ratios on earthquake magnitude and source-to-site distance for the strike-slip case was studied by binning the records in three groups of magnitudes and three groups of distances. The mean ratios of each group are presented in Figure 5, which shows that the ratios are relatively insensitive to source-to-site distance but have a moderate dependence on magnitude. However, there seems to be no clear trend on how these variables affect the ratios.

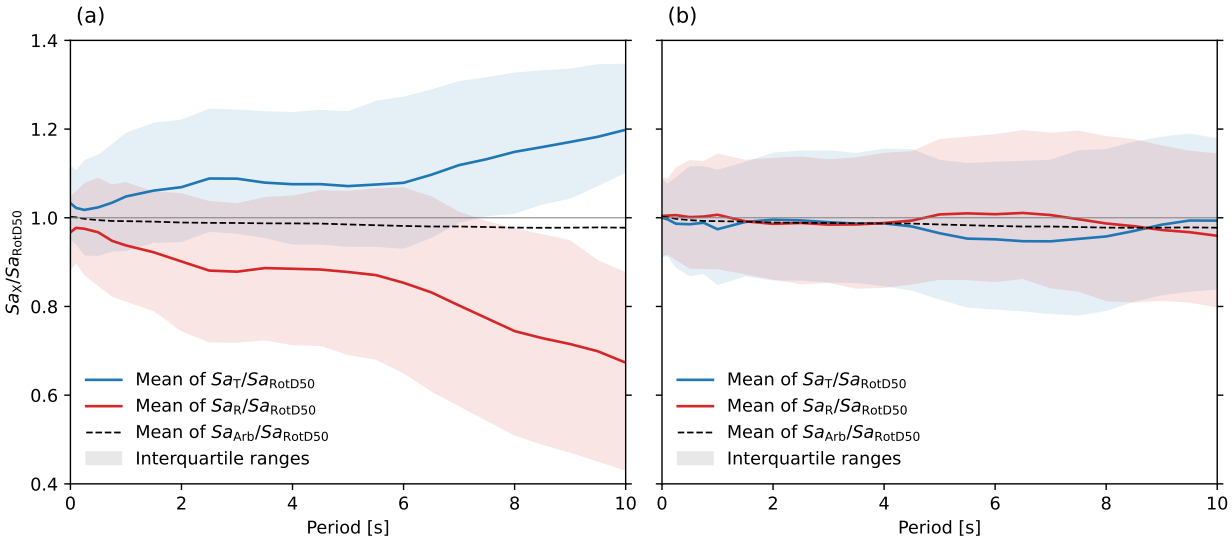

Figure 4: Mean ratios between spectral accelerations in the transverse or radial orientations and the RotD50 spectral acceleration for ground motions from (a) strike-slip and (b) reverse earthquakes.

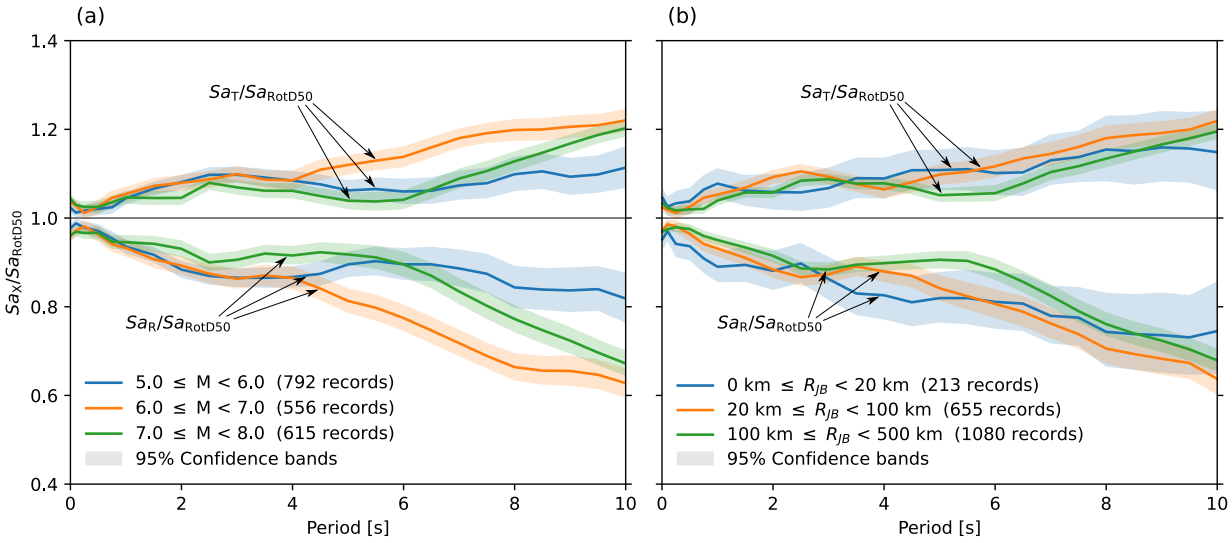

Figure 5: Dependence of mean Sa_T/Sa_{RotD50} and Sa_R/Sa_{RotD50} ratios of records from strike-slip earthquakes on (a) earthquake magnitude and (b) source-to-site distance.

Because several previous studies have assumed that spectral accelerations in the strike-normal orientation are larger than average (e.g., Somerville et al., 1997), comparing them with those in the transverse orientation studied in this work is of interest. Figure 6 compares the ratios between spectral accelerations in the transverse orientation and the orientation-independent RotD50 intensity (Sa_T/Sa_{RotD50}) with the ratios between spectral acceleration in the strike-normal orientation and the RotD50 intensity (Sa_{SN}/Sa_{RotD50}) for three periods. The transverse orientation ratios were computed only for records from strike-slip earthquakes, whereas the strike-normal orientation ratios were computed for all selected records because the model proposed by Somerville et al. (1997)

applies to both styles of faulting. The distributions of rupture distances in each ground motion set are given by the histograms on the top of Figure 6, which change with periods because of the maximum usable periods of the records. The general trend of both ratios with rupture distance is presented using locally weighted scatterplot smoothing (LOWESS, Cleveland, 1979), computed by locally weighted linear regressions that used 20% of the data points whose rupture distances were closest to each point. At all distances and periods, the LOWESS trends of $Sa_{\mathrm{T}}/Sa_{\mathrm{RotD50}}$ are larger than $Sa_{\mathrm{SN}}/Sa_{\mathrm{RotD50}}$ and the difference between them usually becomes more significant as the period and rupture distance increase. This suggests that ground motion directionality is probably better characterized as a function of the angular distance with respect to the transverse orientation than to the strike-normal orientation. The trend even holds for distances to the rupture less than 20 km, where one could perhaps expect $Sa_{\mathrm{SN}}/Sa_{\mathrm{RotD50}}$ ratios to be larger than $Sa_{\mathrm{T}}/Sa_{\mathrm{RotD50}}$ ratios due to directivity effects in the near field. Moreover, $Sa_{\mathrm{T}}/Sa_{\mathrm{RotD50}}$ remains relatively stable throughout the distance range and increases as the period becomes longer, whereas $Sa_{\mathrm{SN}}/Sa_{\mathrm{RotD50}}$ tends to decrease as the rupture distance increases, especially for long-period oscillators. Figure 6 also presents 95% pointwise confidence bands computed using bootstrapping (Efron and Tibshirani, 1993).

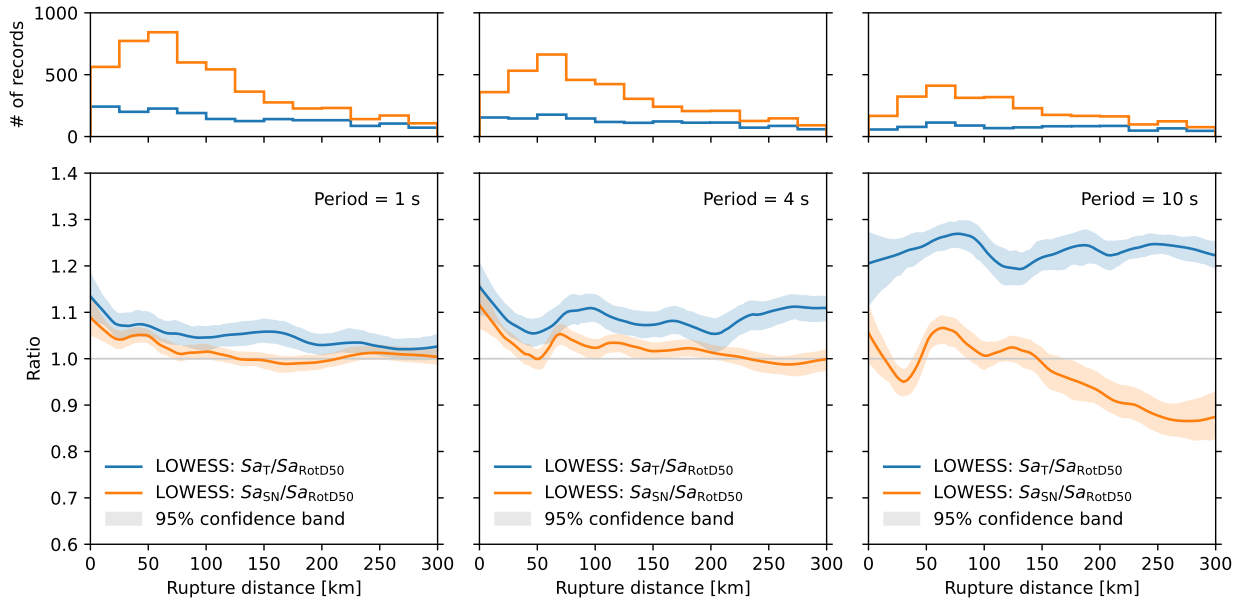

Figure 6: Locally weighted scatterplot smoothing (LOWESS) of the $Sa_{\mathrm{T}}/Sa_{\mathrm{RotD50}}$ and $Sa_{\mathrm{SN}}/Sa_{\mathrm{RotD50}}$ ratios as a function of rupture distance for oscillators with periods of (a) 1 s, (b) 4 s, and (c) 10 s.

Estimation of spectral responses in any given horizontal orientation

The previous section dealt with spectral accelerations in the transverse and radial orientations. However, the orientation of interest does not necessarily coincide with these two orientations.

Thus, the spectral accelerations in the horizontal plane from strike-slip ground motions were also studied as a function of their angular difference to the transverse orientation ($\tilde{\theta}$) in the [-90°,90°] range, which covers all possible orientations. These orientation-specific spectral accelerations, $Sa(\tilde{\theta})$, were normalized by their associated orientation-independent RotD50 intensities, and their means, geometric means, and interquartile ranges (shaded regions) are shown in Figure 7 for periods of 1, 4, and 10 s. The left and right panels of Figure 7 show these statistics in Cartesian and polar coordinate systems, respectively. As expected, on average, the maximum and minimum spectral accelerations occur very close to the transverse ($\tilde{\theta} = 0°$) and radial ($\tilde{\theta} \in \{-90°, 90°\}$) orientations, respectively. Moreover, the variation with angle becomes more significant as the period increases, which agrees with the results in the radial and transverse orientations (see Figures 3 and 4).

A model was developed to transform the mean and standard deviation of the logarithm of a RotD50 spectral acceleration, usually given by modern GMMs, to equivalent statistics associated with a spectral acceleration at any specific orientation. Because, as shown in Figure 7, the statistics of the $Sa(\tilde{\theta})/Sa_{\text{RotD50}}$ ratio are almost symmetric with respect to $\tilde{\theta} = 0°$, the model was developed assuming these ratios as perfectly symmetric with respect to the transverse orientation, that is, they are computed as a function of $\theta = |\tilde{\theta}|$. In other words, the model treats in the same way orientations that are clockwise and counterclockwise from the transverse orientation. To simplify the notation, the ratio between a spectral acceleration at a given angular distance to the transverse orientation, $Sa(\theta)$, and Sa_{RotD50} is defined as:

$$\gamma(\theta) \equiv \frac{Sa(\theta)}{Sa_{\text{RotD50}}} \tag{1}$$

The mean logarithm of the orientation-independent Sa_{RotD50} intensity can then be transformed into the mean logarithm of a spectral acceleration at any given orientation with respect to the transverse orientation, $Sa(\theta)$, using:

$$\text{E}\left[\ln Sa(\theta)\right] = \text{E}\left[\ln Sa_{\text{RotD50}}\right] + \underbrace{\text{E}\left[\ln \gamma(\theta)\right]}_{\ln \mu(\theta)} \tag{2}$$

which requires knowing the geometric mean of the ratio between both quantities, $\mu(\theta)$. In Equation (2), E[·] represents the expectation function, and hence $\text{E}\left[\ln Sa_{\text{RotD50}}\right]$ corresponds to the mean of the natural logarithm of RotD50, usually given by most recent GMMs. The geometric mean, $\mu(\theta)$, is represented by the solid lines of Figure 8, which are shown as a function of θ for different periods (Figure 8a) and as a function of period for the transverse and radial orientations (Figure 8b). As expected, $\mu(\theta)$ varies more with changes in angle θ as the period increases.

To simplify the use of these results, the following model was fitted through regression analysis to the geometric mean ratios for each period independently:

$$\hat{\mu}(\theta) = C_1 + C_2 \cos(2\theta) + C_3 \cos(4\theta) \tag{3}$$

where C_1, C_2, and C_3 are fitted parameters of the model. The resulting regression model is also shown with dashed lines in Figure 8 to compare with the empirical statistical results computed with the NGA-West2 recorded ground motions. After considering several functional forms, Equation (3) was selected because it fits the data extremely well while minimizing the number of parameters.

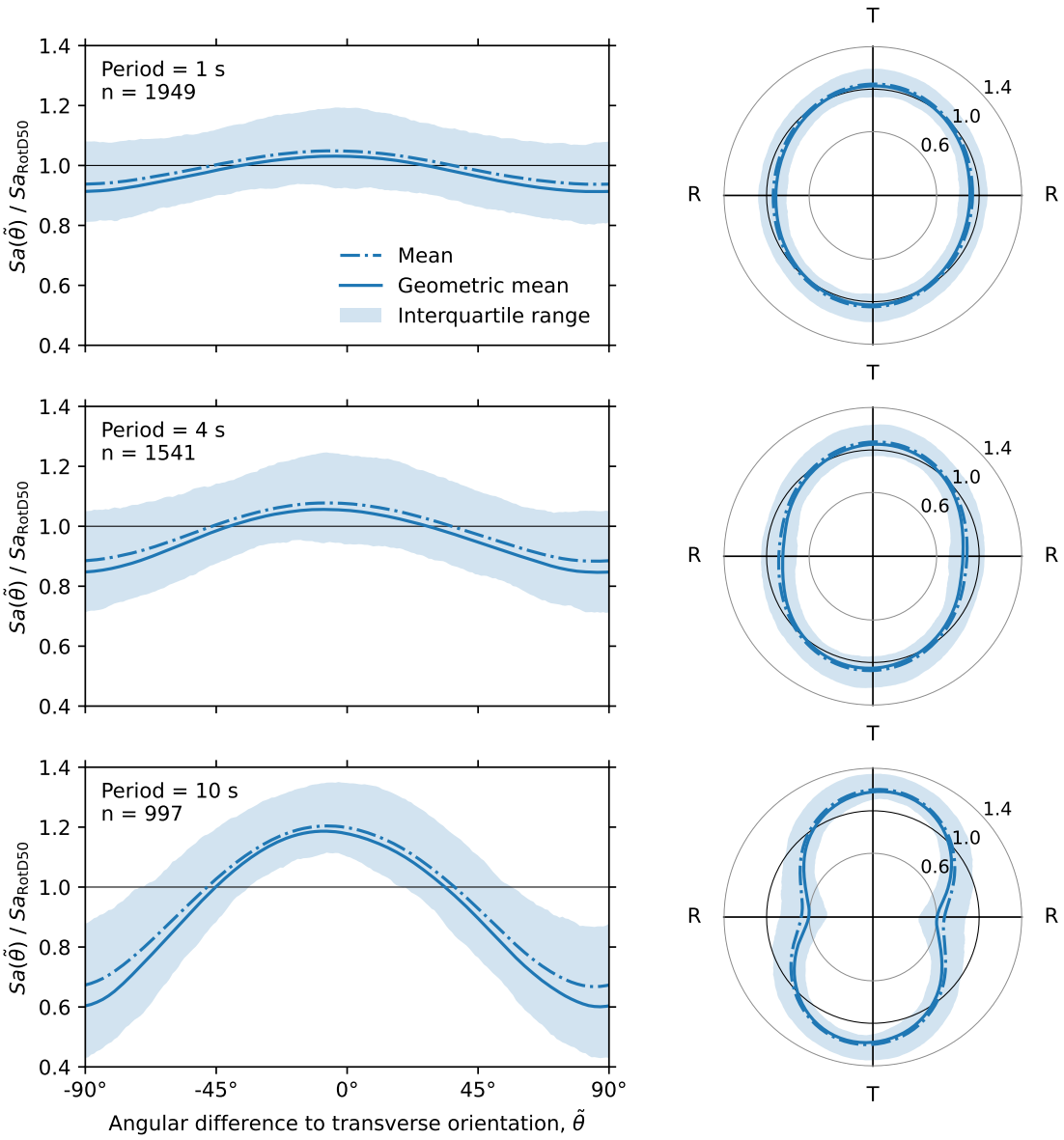

Figure 7: Ratios between spectral acceleration at a given angle $\tilde{\theta}$ from the transverse orientation and the orientation-independent RotD50 intensity of records from strike-slip earthquakes for oscillators with periods of 1, 4, and 10 s. The period of the oscillator and number of records (n) are given within each panel.

The logarithmic standard deviation of the orientation-independent RotD50 spectral acceleration, $\sigma\left[\ln Sa_{\mathrm{RotD50}}\right]$, can be transformed into the logarithmic standard deviation of a spectral acceleration at any orientation, $\sigma\left[\ln Sa(\theta)\right]$, by using the following equation of the orientation-specific variance:

$$\sigma^2\left[\ln Sa(\theta)\right] = \sigma^2\left[\ln Sa_{\mathrm{RotD50}}\right] + \underbrace{\sigma^2\left[\ln \gamma(\theta)\right]}_{\sigma^2(\theta)} + 2\,\mathrm{Cov}\left[\ln Sa_{\mathrm{RotD50}}, \ln \gamma(\theta)\right] \tag{4}$$

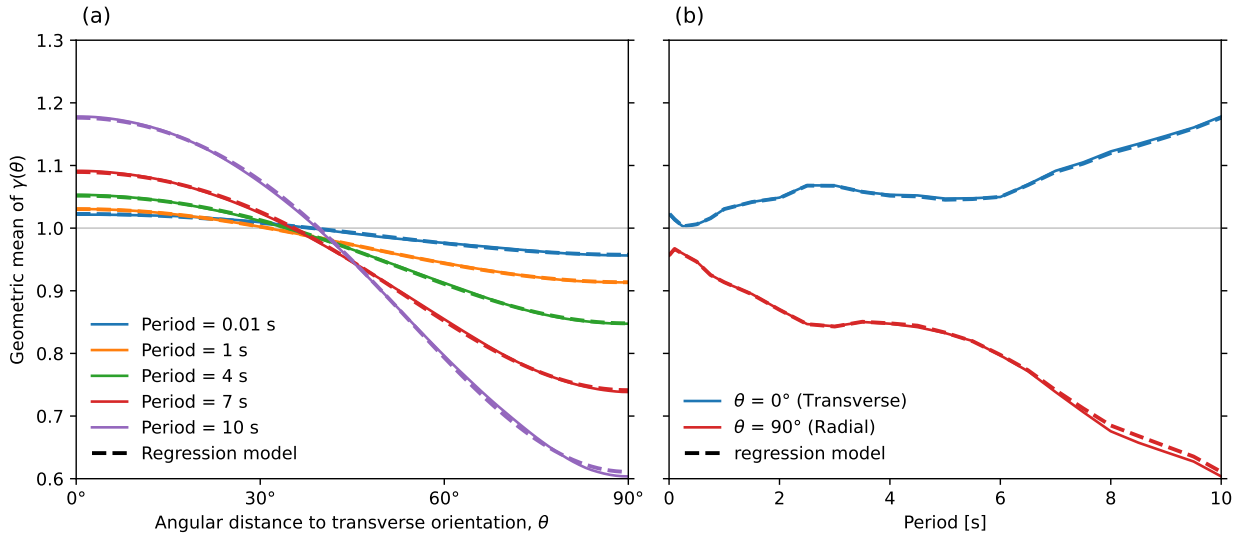

Figure 8: Geometric mean of the ratio between spectral acceleration at given angles θ from the transverse orientation and the RotD50 intensity as a function of (a) angle θ and (b) period. Dashed lines correspond to the fitted regression model. All considered ground motions are from strike-slip earthquakes.

where $\sigma[\cdot]$ represent the standard deviation and $\mathrm{Cov}[\cdot,\cdot]$ represents the covariance:

$$\mathrm{Cov}\left[\ln Sa_{\mathrm{RotD50}}, \ln\gamma(\theta)\right] = \underbrace{\mathrm{Corr}\left[\ln Sa_{\mathrm{RotD50}}, \ln\gamma(\theta)\right]}_{\rho(\theta)} \sigma\left[\ln Sa_{\mathrm{RotD50}}\right] \underbrace{\sigma\left[\ln\gamma(\theta)\right]}_{\sigma(\theta)} \tag{5}$$

and $\mathrm{Corr}[\cdot,\cdot]$ represents the correlation. As shown in Equations (4) and (5), the computation of the logarithmic standard deviation at a specific orientation requires two quantities, the standard deviation of $\ln\gamma(\theta)$ and the correlation between $\ln Sa_{\mathrm{RotD50}}$ and $\ln\gamma(\theta)$, which are denoted here for simplicity as $\sigma(\theta)$ and $\rho(\theta)$, respectively. These two quantities are presented in Figure 9 using solid lines as a function of angle θ between the orientation of interest and the transverse orientation for different periods. The $\rho(\theta)$ correlations were computed using residuals with respect to the GMM developed by Boore et al. (2014). Using three other GMMs also developed with the NGA-West2 database (e.g., Abrahamson et al., 2014; Campbell and Bozorgnia, 2014; Chiou and Youngs, 2014) resulted in fairly similar correlations.

The following models were fitted using nonlinear regression analysis to $\sigma(\theta)$ and $\rho(\theta)$ for each period independently:

$$\hat{\sigma}(\theta) = C_4 + C_5 \exp\left(-C_6(\theta - \pi/2)^2\right) \tag{6}$$

$$\hat{\rho}(\theta) = C_7 + C_8 \cos(2\theta) \tag{7}$$

where C_4 - C_8 are fitted parameters of the models, and θ is in radians. The models are shown by dashed lines in Figure 9 for five periods and are very close to the empirical data. The fitted parameters for 32 periods between 0.01 and 10 s are available in the supplemental material to this article.

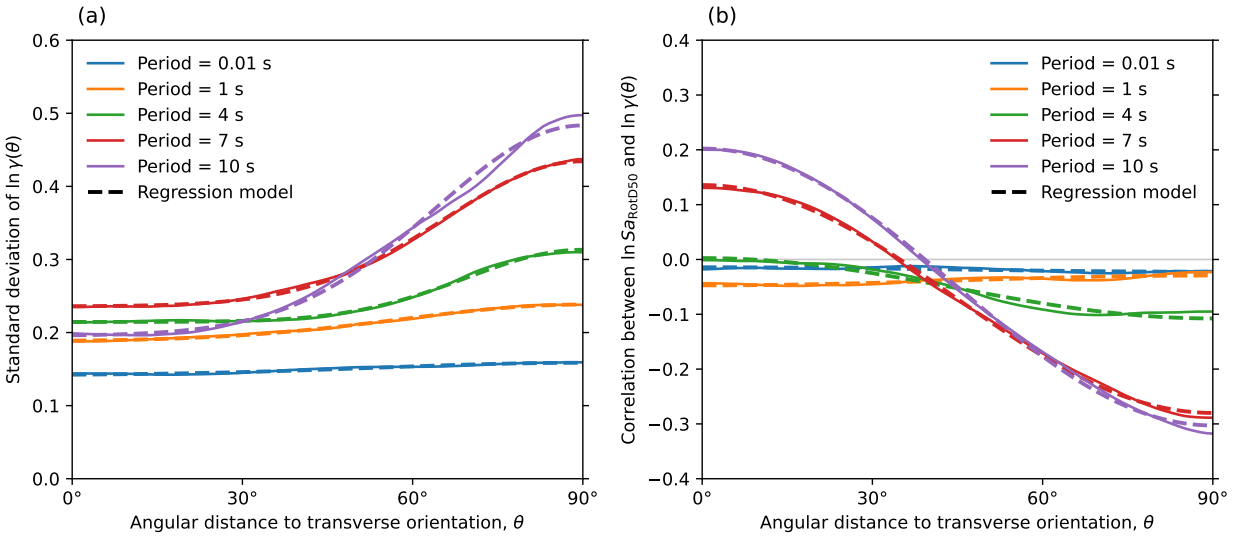

Figure 9: (a) Standard deviation of $\ln \gamma(\theta)$ and (b) correlation between $\ln Sa_{\text{RotD50}}$ and $\ln \gamma(\theta)$, as a function of angle θ. Dashed lines correspond to the fitted regression model. All considered ground motions are from strike-slip earthquakes.

Using of the model given by Equations (2)-(7) is relatively straightforward. For a spectral acceleration in a given orientation (azimuth) at a given site generated by a strike-slip earthquake with a given epicenter, the steps to modify the outputs of a GMM developed for RotD50 are:

1. Compute the transverse orientation at the site of interest using the locations of the site and the earthquake epicenter.
2. Calculate the angular distance $\theta \in [0°, 90°]$ between the orientation of interest and the transverse orientation.
3. Compute $\mu(\theta)$, $\sigma(\theta)$, and $\rho(\theta)$ using Equations (3), (6), and (7), respectively.
4. Obtain the mean and standard deviation of $\ln Sa_{\text{RotD50}}$ using a GMM.
5. Modify the mean and standard deviation by using Equation (2) and by taking the square root of Equation (4), respectively.

To exemplify the use of the model, Figure 10 shows how the standard deviation of the GMM developed by Boore et al. (2014) changes when applied to the transverse and radial orientations for cases when the earthquake magnitude is ≥ 5.5, the Joyner-Boore distance (R_{JB}) is ≤ 78 km, and V_{S30} is ≥ 300 m/s (the GMM standard deviations are constant in these cases). As expected, the modifications to the standard deviation are very minor at periods shorter than roughly 0.5 s because θ is not a good predictor of the orientation of RotD100 at these periods. At longer periods, the modifications are more significant and depend on the orientation of interest. Figure 10 also shows separate curves for the cases when the correlation term, $2\rho(\theta)\sigma[\ln Sa_{\text{RotD50}}]\sigma(\theta)$, is considered and is not considered when modifying the standard deviations. The correlation term is clearly significant at long periods, especially for the radial orientation, for which it reduces the standard

deviation significantly. For the transverse orientation, considering the correlation term increases the standard deviation at long periods, although the effect is relatively minor. The correlation values are affected by the fact that the statistics of the γ ratio do not depend on the predictor variables usually used in GMMs, such as earthquake magnitude and source-to-site distance. If such a model were developed, the correlations could be computed with the residuals with respect to the model. Although, a better solution to estimate spectral ordinates in future strike-slip earthquakes could be to develop a GMM that depends on θ directly; thus, the modification proposed here would not be required.

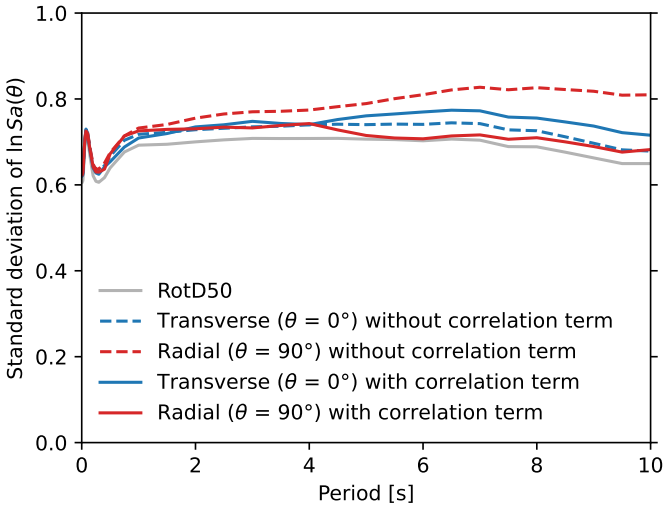

Figure 10: Standard deviations of $\ln Sa(\theta)$ as a function of period obtained by modifying the Boore et al. (2014) GMM for cases when $M_w \geq 5.5$, $R_{JB} \leq 78$ km, and $V_{S30} \geq 300$ m/s. The standard deviations are computed with and without considering the covariance term of Equation (4) for the transverse ($\theta = 0°$) and radial ($\theta = 90°$) cases.

If complete probability distributions of the γ ratios are required, the data shows they can be well represented by scaled beta distributions with the following probability density function:

$$f_\Gamma(\gamma) = \begin{cases} \dfrac{(\gamma)^{\alpha-1}(\sqrt{2}-\gamma)^{\beta-1}}{(\sqrt{2})^{\alpha+\beta-1}B(\alpha,\beta)} & \text{if } \gamma \in [0,\sqrt{2}] \\ 0 & \text{if } \gamma \notin [0,\sqrt{2}] \end{cases} \tag{8}$$

where Γ is a scaled beta distributed random variable, α and β are the shape parameters of the distribution, and $B(\cdot,\cdot)$ is the beta function. The minimum and maximum values of the distribution are 0 and $\sqrt{2}$, respectively, because these correspond to the lower and upper bounds of γ. The scaled beta distribution was fitted to γ ratios at different periods and values of angle θ. The fitted distribution parameters are presented in the electronic supplement to this article, together with a comparison between empirical and fitted distributions in Figure S1.

Conclusions

This paper presents a horizontal ground motion directionality model for strike-slip earthquakes to predict spectral accelerations at any given orientation (azimuth). Spectral accelerations were found to be higher than average in the transverse orientation, that is, the orientation that is perpendicular to the direction at the site that points towards the earthquake epicenter, and lower than average in the radial orientation (i.e., perpendicular to the transverse orientation and pointing towards the epicenter). These differences become more important as the period increases. Moreover, spectral accelerations in the transverse orientation were found to be, on average, larger than those in the strike-normal orientation, which previous studies have usually assumed to be the orientation of maximum intensity because of directivity effects.

Spectral accelerations, on average, increase as the orientation of interest approaches the transverse orientation. Thus, simple analytical expressions that depend on the angular distance between these orientations (i.e., transverse and orientation of interest) were developed and fitted to transform the mean and standard deviation of the logarithm of orientation-independent RotD50 intensities at a site into equivalent statistics for a spectral acceleration at any fixed orientation of interest. These empirical expressions depend on the period and the angle between the orientation of interest and the transverse orientation. The model developed in this study can be used to modify outputs from GMMs derived to estimate RotD50 intensities and obtain a probability distribution for spectral accelerations at any given azimuth. These distributions could, for example, be used to estimate spectral accelerations at fixed azimuths for a given earthquake scenario and in probabilistic seismic hazard analyses.

The proposed model has several limitations. First, other than the period, the regression models do not depend on predictor variables usually used in GMMs, such as magnitude and source-to-site distance. However, the effect of source-to-site distance was found to be minor, and the effect of magnitude was moderate, although no clear trend was identified. Moreover, the effect of site conditions on directionality was not studied. Furthermore, because the model was developed for shallow crustal earthquakes, its applicability to other tectonic regimes, such as subduction earthquakes, requires further studies. Finally, using the epicenter of very large earthquakes to define the transverse orientation at sites close to the source might lead to significant errors, especially when the hypocenter is far from the location where most of the slip occurs (e.g., the 2002 M_w 7.9 Denali earthquake).

Although the model presented in this study is for 5%-damped spectral accelerations, it could be easily extended to consider other damping ratios or ground motion intensity measures, such as filtered incremental velocity (Dávalos and Miranda, 2019), which has been found to be better correlated with structural collapse of buildings. Moreover, the model could also be developed to modify GMMs that use definitions of the horizontal component other than RotD50, such as the geometric mean of the two as-recorded components or GMRotI50 (Boore et al., 2006).

Data and Resources

The ground motion records from the 2019 M_w 7.1 Ridgecrest earthquake, which were only used for Figure 1, were obtained from the Center for Engineering Strong Motion Data (https://doi.org/10.5066/P9REBW60). All other ground motion records used in this study were obtained from

the NGA-West2 ground motion database developed by the Pacific Earthquake Engineering Research Center (https://ngawest2.berkeley.edu/spectras/new, last accessed April 2020). The maps of Figure 1 used tiles by Stamen Design, under CC BY 3.0, and basemap data by OpenStreetMap, under ODbL. The supplemental material includes beta distributions fitted to the γ ratios and the fitted parameters for Equations (3), (6), and (7). The supplemental material also includes figures showing the number of usable records and earthquakes as a function of period, and a map with the orientations of RotD100 for the 2019 M_w 6.4 Ridgecrest earthquake.

Acknowledgments

The authors would like to thank the National Agency for Research and Development (ANID) / Doctorado Becas Chile / 2019-72200307, the Nancy Grant Chamberlain Fellowship at Stanford University, and the EERI/FEMA NEHRP Graduate Fellowship for sponsoring the doctoral studies of the first author. The authors are also grateful to the various agencies responsible for installing and maintaining seismic recording stations, and to the Pacific Earthquake Engineering Research Center for collecting, processing, and distributing the ground motion records within the NGA-West2 database.

References

Abrahamson, N. A., W. J. Silva, and R. Kamai (2014). Summary of the ASK14 ground motion relation for active crustal regions, *Earthquake Spectra* **30**, 1025–1055.

Ancheta, T. D., R. B. Darragh, J. P. Stewart, E. Seyhan, W. J. Silva, B. S.-J. Chiou, K. E. Wooddell, R. W. Graves, A. R. Kottke, D. M. Boore, T. Kishida, and J. L. Donahue (2014). NGA-West2 database, *Earthquake Spectra* **30**, 989–1005.

Bonamassa, O. and J. E. Vidale (1991). Directional site resonances observed from aftershocks of the 18 October 1989 Loma Prieta earthquake, *Bulletin of the Seismological Society of America* **81**, 1945–1957.

Boore, D. M. (2010). Orientation-independent, nongeometric-mean measures of seismic intensity from two horizontal components of motion, *Bulletin of the Seismological Society of America* **100**, 1830–1835.

Boore, D. M., J. P. Stewart, E. Seyhan, and G. M. Atkinson (2014). NGA-West2 equations for predicting PGA, PGV, and 5% damped PSA for shallow crustal earthquakes, *Earthquake Spectra* **30**, 1057–1085.

Boore, D. M., J. Watson-Lamprey, and N. A. Abrahamson (2006). Orientation-independent measures of ground motion, *Bulletin of the Seismological Society of America* **96**, 1502–1511.

Campbell, K. W. and Y. Bozorgnia (2014). NGA-West2 ground motion model for the average horizontal components of PGA, PGV, and 5% damped linear acceleration response spectra, *Earthquake Spectra* **30**, 1087–1115.

Chiou, B. S.-J. and R. R. Youngs (2014). Update of the Chiou and Youngs NGA model for the average horizontal component of peak ground motion and response spectra, *Earthquake Spectra* **30**, 1117–1153.

Cleveland, W. S. (1979). Robust locally weighted regression and smoothing scatterplots, *Journal of the American statistical association* **74**, 829–836.

Dávalos, H. and E. Miranda (2019). Filtered incremental velocity: A novel approach in intensity measures for seismic collapse estimation, *Earthquake Engineering & Structural Dynamics* **48**, 1384–1405.

Efron, B. and R. J. Tibshirani (1993). *An introduction to the bootstrap*. Chapman & Hall, New York.

Heresi, P., J. Ruiz-García, O. Payán-Serrano, and E. Miranda (2020). Observations of Rayleigh waves in Mexico City Valley during the 19 September 2017 Puebla–Morelos, Mexico earthquake, *Earthquake Spectra* **36**, 62–82.

Hong, H. P. and K. Goda (2007). Orientation-dependent ground-motion measure for seismic-hazard assessment, *Bulletin of the Seismological Society of America* **97**, 1525–1538.

Howard, J. K., C. A. Tracy, and R. G. Burns (2005). Comparing observed and predicted directivity in near-source ground motion, *Earthquake Spectra* **21**, 1063–1092.

Poulos, A. and E. Miranda (2022a). Probabilistic characterization of the directionality of horizontal earthquake response spectra, *Earthquake Engineering & Structural Dynamics* **51**, 2077–2090.

Poulos, A. and E. Miranda (2022b). Proposal of orientation-independent measure of intensity for earthquake-resistant design, *Earthquake Spectra* **38**, 235–253.

Poulos, A. and E. Miranda (2023). Effect of style of faulting on the orientation of maximum horizontal earthquake response spectra, *Bulletin of the Seismological Society of America*. Advance online publication.

Poulos, A., E. Miranda, and J. W. Baker (2022). Evaluation of earthquake response spectra directionality using stochastic simulations, *Bulletin of the Seismological Society of America* **112**, 307–315.

Rekoske, J. M., E. M. Thompson, M. P. Moschetti, M. G. Hearne, B. T. Aagaard, and G. A. Parker (2020). The 2019 Ridgecrest, California, earthquake sequence ground motions: Processed records and derived intensity metrics, *Seismological Research Letters* **91**, 2010–2023.

Shahi, S. K. and J. W. Baker (2014). NGA-West2 models for ground motion directionality, *Earthquake Spectra* **30**, 1285–1300.

Somerville, P. G., N. F. Smith, R. W. Graves, and N. A. Abrahamson (1997). Modification of empirical strong ground motion attenuation relations to include the amplitude and duration effects of rupture directivity, *Seismological Research Letters* **68**, 199–222.

Spudich, P., M. Hellweg, and W. H. K. Lee (1996). Directional topographic site response at Tarzana observed in aftershocks of the 1994 Northridge, California, earthquake: implications for mainshock motions, *Bulletin of the Seismological Society of America* **86**, S193–S208.

Watson-Lamprey, J. A. and D. M. Boore (2007). Beyond Sa_{GMRotI}: Conversion to Sa_{Arb}, Sa_{SN}, and Sa_{MaxRot}, *Bulletin of the Seismological Society of America* **97**, 1511–1524.